NACA

RESEARCH MEMORANDUM

SIMULATOR STUDIES OF A SIMPLE HOMING SYSTEM

By Anthony L. Passera and H. Douglas Garner

Langley Aeronautical Laboratory
Langley Field, Va.

NATIONAL ADVISORY COMMITTEE
FOR AERONAUTICS

WASHINGTON

October 6, 1955
Declassified December 1, 1959

NATIONAL ADVISORY COMMITTEE FOR AERONAUTICS

RESEARCH MEMORANDUM

SIMULATOR STUDIES OF A SIMPLE HOMING SYSTEM

By Anthony L. Passera and H. Douglas Garner

SUMMARY

Simulator studies were conducted of a simple homing missile pursuing a constant-velocity nonmaneuvering target. The missile dynamics in pitch and roll, the seeker method of detection and control, and the missile-target geometry were simulated to determine whether the method of control and detection in conjunction with the missile dynamics were feasible. These studies did indicate that the operation and principles of the simple homing system were feasible. The simulation studies also yielded the firing conditions necessary for a pursuit collision course. Plots were made from these studies that give the missile firing ranges for a pursuit collision course as a function of the initial missile-target bearing angle.

INTRODUCTION

The accuracy of present-day-aircraft rocket armament is hampered by factors such as launching errors and random dispersion. This accuracy might be improved by the incorporation of some sort of simple homing device that would reduce these errors and dispersion. The principles of operation of one such homing system were described in reference 1. The function of this seeker with its contactor-servo characteristics is to make small corrections in the flight path, holding the rocket on approximately a pursuit navigation course. The seeker controls the pitching and rolling performance of the missile by means of fixed deflections on the pitch control surfaces and servo-actuated roll control surfaces. Reliability in performance of the control and detection systems is made as high as possible by making these systems simple. In order to determine the feasibility of such a homing system, simulator studies of the performance of the seeker and rocket-motor combination were considered necessary. The simulator studies were carried out with the aid of two simulators: a qualitative and a quantitative simulator. The qualitative simulator gave an indication of the problems involved in the proposed guidance system, whereas the quantitative simulator indicated what effect various system parameters had on the ability of the missile to remain on a pursuit collision course. These studies were performed on the simple homing missile

in a pursuit navigation system with a constant velocity nonmaneuvering
target. The missile-to-target velocity ratio was 2.

SYMBOLS

K roll-dynamics velocity constant, $\dfrac{\dot{\phi}_0}{\delta_r}$, deg/sec/deg

$b = 2\zeta\omega_n$

K_g tachometer constant

K_p velocity constant of two-phase motor

K_1 $\omega_n^2 \times$ Position constant of airframe transfer function α/δ,
                 deg/deg

K_2 longitudinal-motion velocity constant, $\dot{\gamma}/\alpha$, deg/sec/deg

M Mach number

O origin of Cartesian coordinate system employed in missile-
                 target geometry

r turning radius, ft

R range along line of sight between missile and target, ft

S Laplace transform variable

V velocity along flight path, ft/sec

W.B.   wheel base of qualitative simulator, ft

x,y,z space axes of Cartesian coordinates

α angle of attack of missile, deg

β angle subtended by missile-target line of sight and missile
                 velocity vector, deg

γ flight-path angle measured from horizontal, deg

δ pitch or roll canard control-surface deflection, deg

ϵ error angle of roll control system, angle between ϕ_i- and ϕ_o-planes, deg

ζ damping ratio

η bearing angle subtended by missile-target line of sight and target velocity vector, deg

σ angle subtended by missile-target line of sight and horizontal, deg

τ time constant of missile roll dynamics, sec

τ_p time constant of two-phase motor, sec

ϕ_i roll reference for roll control system; defined as plane determined by missile longitudinal axis and target position

ϕ_i',ϕ_o' angles between ϕ_i- and ϕ_o-planes and arbitrary reference plane

ϕ_o plane defined by axis of detector and longitudinal axis of missile

ω_n undamped natural frequency of missile longitudinal motion, radians/sec

Subscripts:

x   motion in z-x plane

y   motion in x-y plane

M   motion associated with missile

p   constants associated with two-phase motor

T   motion associated with target

s   motion associated with qualitative simulator

r   roll control-surface deflection

A dot over a symbol indicates first derivative with respect to time.

DESCRIPTION OF GUIDANCE AND CONTROL SYSTEM

The purpose of the missile control and guidance system described in this paper is to hold the rocket on approximately a pursuit navigation course by discontinuously reducing the error between the missile-target line of sight and the missile resultant velocity vector. While the missile is flying directly toward the target, the missile rolls freely; however, the fixed pitch canard deflection shown in figure 1 causes the missile to fly in a helical path with its resultant velocity vector directed toward the target. During the free-rolling performance of the missile, the missile-target line of sight lies within the center dead cone described by the inner edge of the pitch-plane field of view. This pitch-plane field of view is the instantaneous field of view of the detector while the missile is hunting in roll or rolling freely. As the missile-target line of sight moves outside the limits of this center cone, the detector senses the target position and calls for a reverse roll torque on the nose section each time that the pitch-plane field of view coincides with the ϕ_i-plane. As a result of lags due to the roll-control-system time constant and the roll-servo actuating time, the missile hunts in roll about the ϕ_i-plane, with the resultant lift lying in this plane. The missile corrects its flight path as a result of this hunting oscillation, causing the missile-target line of sight to move until it lies again within the previously mentioned dead cone. Then the missile rolls freely and is flying directly toward the target. The missile will continue to roll freely until this sequence is repeated, as a result of the line of sight having moved beyond the limits of the aforementioned cone.
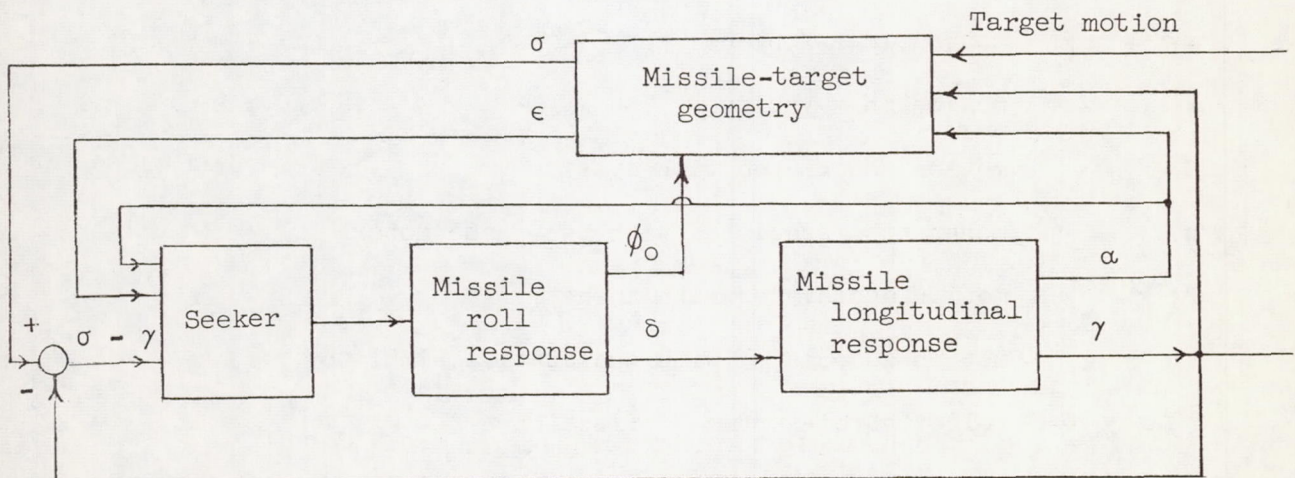
This diagram shows that the seeker responds to the error signal $\sigma - \gamma$; however, the other inputs ϵ and α are necessary for the seeker to

sense the roll-angle reference of the target, thus enabling the missile
to correct the flight path in the proper direction. Since the detector
axis and the lift due to the pitch canard deflection δ lie in the
ϕ_0-plane and have the same sense, δ causes the missile to correct its
flight path properly since α and γ of the longitudinal response,
except for small dynamic lags, have the same sense as δ. The missile-
target-geometry block with its inputs gives the orientation of the line
of sight with respect to the missile velocity vector.

Simple Homing Missile

In order to mechanize the system concept, the missile shown in fig-
ure 3 was designed to be aerodynamically capable of carrying out the
required functions. This is not the only suitable aerodynamic configura-
tion nor necessarily the most efficient; nevertheless, the configuration
was chosen for the purpose of this study.

The fuselage consists of two sections coupled with a bearing, which
permits each section to rotate freely with respect to the other. The
rear section contains the rocket motor, rear stabilizing surfaces, and
space for telemetering equipment. The nose section contains the detector
and associated electronics, two pairs of canard control surfaces, a two-
position pneumatic actuator attached to one pair of control surfaces, and
an air reservoir with regulating devices to power the actuator. One pair
of canard control surfaces is fixed to give lift, in what has been pre-
viously referred to as the pitch plane of the missile. The other pair
of canards is positioned differentially by the actuator to produce either
a positive or negative roll torque on the nose section. The design of
the seeker head is such that the nose section of the missile is roll-
controlled through the roll canard surfaces, which results in the average
lift being positioned as previously discussed. With reference to fig-
ures 1 and 2, this is accomplished by the seeker as it calls for a reverse
roll torque each time the pitch-plane field of view or detector axis coin-
cides with the ϕ_i-plane.

Control-System Transfer Functions

The longitudinal motion of the airframe is described by the following
transfer functions that are based upon a two-degree-of-freedom analysis
with small disturbances from a straight-line constant-velocity course:

$$\frac{\alpha}{\delta}(S) = \frac{K_1}{S^2 + 2\zeta\omega_n S + \omega_n^2}$$

$$\frac{\gamma}{\delta}(S) = \frac{K_1 K_2}{S\left(S^2 + 2\zeta\omega_n S + \omega_n^2\right)}$$

The rolling performance is based upon a single-degree-of-freedom system with small disturbances from any roll reference angle and is described by

$$\frac{\phi_o}{\delta_r}(S) = \frac{K}{S(\tau S + 1)}$$

The values of these coefficients are given in table I.

The response of the seeker and roll control servo to an input command signal is nonlinear; however, the following describing function illustrates the dynamic performance of the seeker and roll control-surface servo combination.
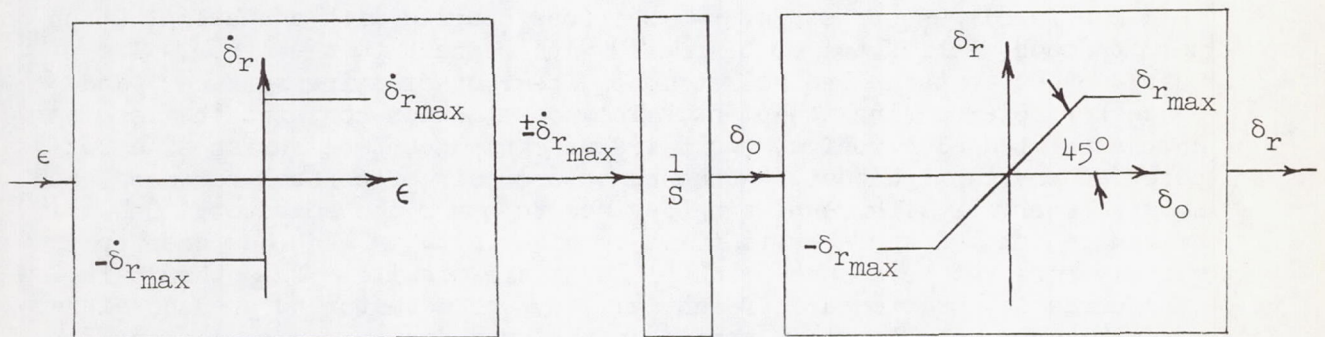
Whenever the planes, ϕ_i and ϕ_o, coincide, the seeker calls for a reverse roll-control-surface deflection. The servo output, in response to the signal from the seeker, travels at saturation speed until full control deflection is attained.

Figure 4 is a block diagram of the roll control system of the missile. Whenever the detector or pitch plane hunts across the ϕ_i-plane, the roll control system is analogous to a contactor-type servomechanism. References 2 and 3 are very useful in determining the hunting frequency and amplitude in roll for the dynamic performance of the missile while it is hunting on the target and correcting its flight path.

Geometry Equations

The missile-target geometry and equations are shown in figure 5. The motions of the missile and target in space are represented by the projections of the missile-target flight angles on the zx- and xy-planes

or the vertical and horizontal planes, respectively. The zx-plane is shown in the figure. The center of gravity of the missile is at the point O, or the intersection of the x-, y-, and z-axes. These two planes are translated through space, with the point O moving along the missile flight path.

PROBLEM SIMULATION

The performance of this simple homing missile was simulated on both the qualitative and the quantitative simulators. Both were designed, primarily, to study the pursuit of a constant-velocity nonmaneuvering target by the missile, with a missile-to-target velocity ratio of 2. The functions of both simulators can be divided into two parts: roll and pitch dynamics of the missile, and tracking geometry.

The first function is performed in somewhat the same manner in both simulators by electromechanical means. The tracking geometry is performed in the qualitative simulator by steering moving carts representing the missile and target, and thereby providing simulation in one plane only. In the quantitative simulator, the tracking geometry is solved by a Reeves Electronic Analog Computer, and motion in space is represented.

Qualitative Simulator

The physical arrangement of the qualitative simulator is shown in figures 6 and 7; a block diagram of the roll-dynamics loop is illustrated in figure 8. The roll dynamics of the missile are simulated by a reversible pneumatic motor controlling the rotation of the seeker head. The gearing, throttling, and pressure of the pneumatic motor are adjusted to duplicate the angular acceleration and steady-state rolling velocity of the missile nose section as closely as possible. A four-way pneumatic valve linked to an actuator reverses the flow of air to the motor to simulate the action of the two-position roll-control-surface servo. The actuator is controlled by the seeker head through suitable electronic circuitry.

The pitching dynamics of the missile are roughly simulated by the arrangement shown in figure 7. The air-motor and seeker-head assembly is mounted in gimbals and is restrained about both axes of freedom by springs and damping devices (a dashpot is used on the horizontal axis, and friction between the drive wheel, attached to the vertical axis, and the floor provided approximately the proper amount of damping for this axis). The fixed pitching moment provided in the missile by a deflected fixed canard surface is simulated by linking the restraining springs to the seeker-head assembly through an eccentric. The throw of the

eccentric is adjusted so that one-half of the included angle of the cone swept through by the center line of the seeker head at a very low rotational velocity is equal to the angle of attack calculated for zero rotational velocity. The drive wheel is attached to the vertical gimbal axis so that the angle the drive wheel makes with the center line of the carriage (see fig. 9) represents the projection of the angle of attack of the missile in the operating plane. As shown in figure 9,

$$r_S = \frac{W.B.}{\sin \alpha}$$

Therefore, for a given flight condition and angle of attack, the turning radius is only a function of the wheel base, since

$$\frac{r_M}{r_S} = \text{Space scale factor}$$

The space scale factor of the simulator is set by the wheel base of the tricycle carriage. A tricycle with a wheel base of 2 feet gives a space scale factor of 350:1. In order to perform the simulation in real time, the velocity scale factor must be the same as the space scale factor. The front wheel was driven at the required velocity by an electric motor.

The seeker head, electronic section, and pneumatic actuator were the actual components designed to be used in the missile. The target shown in figure 6(b) consisted of one or more incandescent lamps mounted on a small motor-driven cart to simulate single or multiple targets.

Both missile and target carts were fitted with solenoid-actuated brush pens driven from a common timer so that a record of their paths could be recorded on a large sheet of paper, the timing breaks in the path lines giving the relative instantaneous positions of the two carts.

Quantitative Simulator

A diagram and a photograph of this simulator are shown in figures 10 and 11. In the schematic diagram of figure 10, the seeker head employed is fundamentally the same as that of the missile, in that the seeker field of view scans a cone such as that described in the system concept. A masked photomultiplier electron tube was employed in this case for high sensitivity in response to the image on the oscilloscope screen. The output pulse from the seeker head is amplified to operate a "flip-flop" and relay. The relay output, through a mechanical time delay simulating the operating time of the control-surface actuator, controls the direction of rotation of the head in such a way as to keep the pitch plane of the seeker head hunting across the image of the target. Figure 12 illustrates

the method of simulating the missiles roll dynamics by utilizing an amplifier, a two-phase motor, and a tachometer. The missile rolling time constant and velocity constant are expressed as functions of the motor and tachometer constants. In the diagram, the motor time constant is determined by the lumped inertia of the system. The roll-dynamics time constant was adjusted by changing the size of the inertia disk (see fig. 10) and the amount of tachometer feedback in the motor drive of the head.

The short-period motion of the missile and the missile-target geometry in both the horizontal and vertical planes are solved on the REAC simultaneously. An electromagnetic component resolver geared to the seeker head was used to produce the horizontal and vertical components of the lift vector to be used as inputs to the two REAC channels. The outputs of the REAC channels representing the horizontal and vertical displacements of the target with respect to the missile axis are fed into the X- and Y-channels of the oscilloscope so that the position of the spot on the oscilloscope screen corresponds to that of the target, as seen from the center line of the seeker head.

Since the frequency response of the servo components in the REAC was limited, a reduced time scale was employed in this simulator. Figure 11 is a photograph of the setup shown in figure 10. The intensity of the spot on the oscilloscope was modulated at an audio frequency, and then the signal detected by the seeker was fed through a narrow bandpass filter to reduce extraneous interference. The units on top of the slotted plate are the resolver, two-phase motor and tachometer, seeker head, and device for the servo time delay. The units under the slotted plate are the resolver, demodulators, and "flip-flop." The amplifier for the cell output and the bandpass filter are on the stand under the table.

ANALYSIS PROCEDURE

Qualitative Simulator

Since the purpose of the qualitative simulator was only to obtain an idea of the problems involved in the proposed guidance system, no accurate measurements were attempted with this apparatus. The target was simply started at various missile-target bearing angles and ranges. The effects of multiple targets were determined by lighting 1, 2, or 3 automobile-headlight-type bulbs; the effect of target size was determined by lighting Lumiline bulbs arranged as sides of an equilateral triangle. Records of the flight paths were obtained from the marking pens on the equipment. Parameters were limited to flight conditions at $M = 1.5$ and sea level. Although the qualitative simulator indicated that the proposed system would work, it was too inflexible to allow many parameter changes and provided motion in only one plane.

Quantitative Simulator

The flight conditions for the quantitative simulator are:

1. Constant missile and target velocities
2. Constant missile and target altitudes
3. Linear pitch and roll aerodynamic derivatives
4. Missile and target at the same altitude
5. Missile velocity vector initially along the line of sight
6. Missile initially rolling at its steady-state rolling velocity
7. Target motion along a straight line.

The dynamics of the missile were set up on the REAC as shown in figure 10. This setup neglects any missile gyroscopic effects and also assumes that the missile pitching dynamic response is based upon the nose and tail section being one rigid unit.

The three-dimensional trajectory equations were simplified by considering the missile-target motion confined to the vicinity of the zx-plane, thereby permitting the following substitutions in the equations of figure 5:

$$V_{M,x} = V_M$$

$$V_{T,x} = V_T$$

$$V_{M,y} = V_M \cos \gamma_{M,x}$$

$$V_{T,y} = V_T \cos \gamma_{T,x}$$

These substitutions resulted from considering the angles $\gamma_{M,y}$ and $\gamma_{T,y}$ to be very small.

Because of computer inaccuracies at the closing phase of the pursuit course, accurate determination of miss distance was difficult. In order to avoid the possibility of obtaining erroneous results, a trajectory was considered to yield a collision of the missile and target whenever the missile flight path became tangent to the target flight path and remained there. This is in keeping with a kinematic study of a pure pursuit navigation system.

During the computer study, the target size and intensity were kept invariant. Each study was initiated with the missile velocity vector along the missile-target line of sight with some initial missile-target bearing angle η. At various missile-target bearing angles, the range (starting at some small value) was increased until a collision was obtained. Data obtained in this manner were then summarized by plotting minimum initial missile-target range against initial bearing angle. This resulted in plots similar to that of figure 13.

RESULTS AND DISCUSSION

Qualitative Simulator

The qualitative simulator indicated that the idea conceived for this type of seeker and method of scanning would work, but because of the space scale factor and the inability to vary parameters with ease, evaluation of miss distance and performance at various flight conditions was difficult. The qualitative simulator did give a physical understanding of the performance and requirements in a short time, an understanding that is not always evident with computer simulation.

Figure 14 is a record that is representative of the flight paths of the qualitative simulator for missile-target bearing angles of 20° and 25° at M = 1.5 and sea level. The trajectories are characteristic of those obtained in a pure pursuit navigation system for a range of velocity ratios, in that the missile must fly in a path that becomes tangent to the target flight path to cause a collision with the target. Figure 15 is a sequence of photographs demonstrating the performance of the qualitative simulator homing in on the target cart.

Multiple targets obtained by lighting 1, 2, or 3 automobile-headlight-type bulbs on the target of figure 6 did not seem to hinder the homing performance of the qualitative simulator. Target size was also varied by using 3 Lumiline bulbs arranged in a triangle, with 1, 2, or 3 of these bulbs lighted. None of these factors seemed to hinder the homing performance of the qualitative simulator. In each case, the qualitative simulator would lock on some target or some portion of the target during the closing phase of the pursuit collision course.

Quantitative Simulator

The results obtained from the quantitative simulator are summarized in figures 16, 17, and 18. These figures give the boundaries for the firing ranges and initial missile-target bearing angles necessary for a pursuit collision course and are to be interpreted in the same manner as

was figure 13. Figure 19 shows the flight paths of the missile and tar-
get for several missile-target bearing angles. These trajectories are
also similar to those obtained from the qualitative simulator. Figure 20
is indicative of the variations in the geometry angles and was obtained
from one of the simulator trials. All of these trials show an almost
linear variation of the line of sight with time.

Table I presents the conditions for the cases computed on the quan-
titative simulator, and the summarized results of the tests will be
reviewed in the ensuing discussion.

Figure 16 shows the results of cases 1 and 2 of table I. The solid
lines on the polar plot of figure 16(a) give the boundary that determines
whether the missile firing conditions will yield a pursuit collision
course. The dashed-curve boundary on this same figure is based upon a
point kinematic study (see ref. 4) of a pursuit navigation system with a
velocity ratio of 2. This analysis is of a missile having the same maxi-
mum static normal acceleration as the simple homing missile flying as a
rigid unit with no roll canard deflection. This figure shows how much
the homing performance of the present missile falls short of ideal
performance.

Figure 16(b) shows the effect of a small angular misalinement of the
detector axis. This effect is small when compared with the configuration
in figure 16(a).

Figure 17 shows the results of cases 3 and 4 in table I. Figure 17(a)
shows that a missile with a larger roll time constant requires a greater
initial range for a pursuit collision course when compared with the mis-
sile configuration of figure 16(a). Figure 17(b) indicates that increasing
the damping of the longitudinal motion reduces the initial firing range at
the larger missile-target bearing angles for a given roll time constant;
however, for case 5, which is not shown, the quadratic damping ratio was
increased to 0.7, with the result that the missile was unable to hit the
target for even an initial missile-target bearing angle of 10°.

For figure 18, the use of two angularly displaced detectors, cases 6
and 7, was conceived as a means of reducing the amplitude of the roll
hunting oscillation. A detector configuration such as shown in the sketch
produces a larger average lift force in the ϕ_i-plane for a given pitch
control-surface deflection, since the reverse-roll-torque command occurs
only when the ϕ_i-plane intersects the axes of the detectors as the plane
moves toward the inside of the acute angle.

Detectors
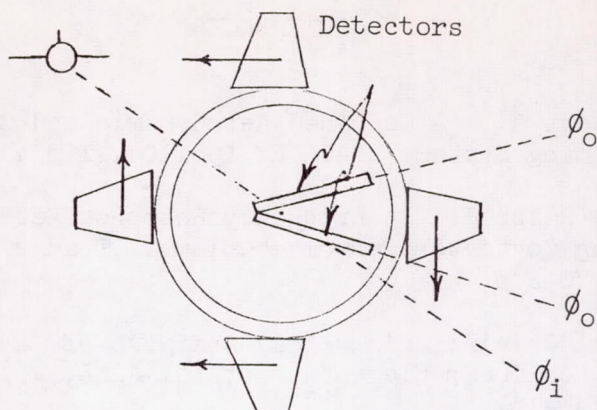
ϕ_o

ϕ_o

ϕ_i

Figure 18 illustrates that two angularly displaced detectors do reduce the initial range for larger bearing angles when compared with figure 16(a).

A change in servo time delay of case 8 showed no significant change in performance over that of case 1. Case 8 is not shown in a figure.

Observations made during the simulator studies indicated that a definite relationship between the angle of attack and the geometry of the optical system must be maintained at all times to prevent the seeker from seeing the target on the wrong side of the missile longitudinal axis, thus preventing the missile from pulling lift in the wrong direction.

CONCLUSIONS

As a result of tests simulating a simple homing missile in a pursuit navigation system with a constant-velocity nonmaneuvering target, and a missile- to target-velocity ratio of 2, the simulator studies indicate that the simple homing missile will perform satisfactorily. Large rolling time constants require greater firing ranges, whereas low pitch damping ratios are required for a collision with a given time constant and roll velocity. Small misalinement of the detector axis did not hinder the homing performance appreciably for any given initial condition. Two angularly displaced detectors improved the performance at the larger initial missile-target bearing angles.

Langley Aeronautical Laboratory,
    National Advisory Committee for Aeronautics,
        Langley Field, Va., June 27, 1955.

REFERENCES

1. Gardiner, Robert A.: A Combined Aerodynamic and Guidance Approach for
   a Simple Homing System. NACA RM L53I10a, 1953.

2. Kochenburger, Ralph J.: A Frequency Response Method for Analyzing and
   Synthesizing Contactor Servomechanisms. Trans. AIEE, vol. 69, pt. I,
   1950, pp. 270-283.

3. Johnson, Ewell Calvin: Sinusoidal Analysis of Feedback Control Systems
   Containing Nonlinear Elements. Trans. AIEE, vol. 71, pt. II, July
   1952, pp. 169-181.

4. Newell, Homer E., Jr.: Guided Missile Kinematics. Rep. No. R-2538,
   Naval Res. Lab., Radio Div., May 22, 1945.

TABLE I

CONDITIONS FOR COMPUTER SIMULATOR AND REAC

Case computed on REAC	Flight condition	Number of cells	Servo time delay, sec	Airframe roll time constant, sec	Steady-state roll velocity, rps	Steady-state angle of attack while missile is rolling at steady-state roll velocity, deg
1	M = 1.2 Sea level	1	0.02	0.04	2.7	4.5
2	M = 1.2 Sea level	1 10° skew	0.02	0.04	2.7	4.5
3	M = 1.2 Sea level	1	0.02	0.12	2.7	4.5
4	M = 1.2 Sea level	1	0.02	0.12	2.7	4.5
5	M = 1.2 Sea level	1	0.02	0.12	2.7	4.5
6	M = 1.2 Sea level	2 at 20°	0.02	0.04	2.7	4.5
7	M = 1.2 Sea level	2 at 10°	0.02	0.04	2.7	4.5
8	M = 1.2 Sea level	1	0.08	0.04	2.7	4.5

TABLE I.- Concluded

CONDITIONS FOR COMPUTER SIMULATOR AND REAC

Case computed on REAC	K_1	ζ	ω_n, radians/sec	K_2, deg/sec/deg	Field of view, deg	Total dead zone, deg
1	541	0.14	29.8	3.4	7	2
2	541	0.14	29.8	3.4	6	2
3	541	0.14	29.8	3.4	6	2
4	541	0.50	29.8	3.4	6	2
5	541	0.70	29.8	3.4	6	2
6	541	0.14	29.8	3.4	8	2
7	541	0.14	29.8	3.4	9	2
8	541	0.14	29.8	3.4	6	2

Pitch-Plane Field of View, ϕ_0

Missile-Target Line of Sight

Roll Control Surfaces

Pitch Control Surface

Target

Mirror

a

V

ϕ_0 ϕ_i

Detector

Center Dead Cone

Bearing for Free-Rolling Head

Missile Longitudinal Axis

Resultant Velocity Vector

Active Cone Scanned by the Seeker Field of View
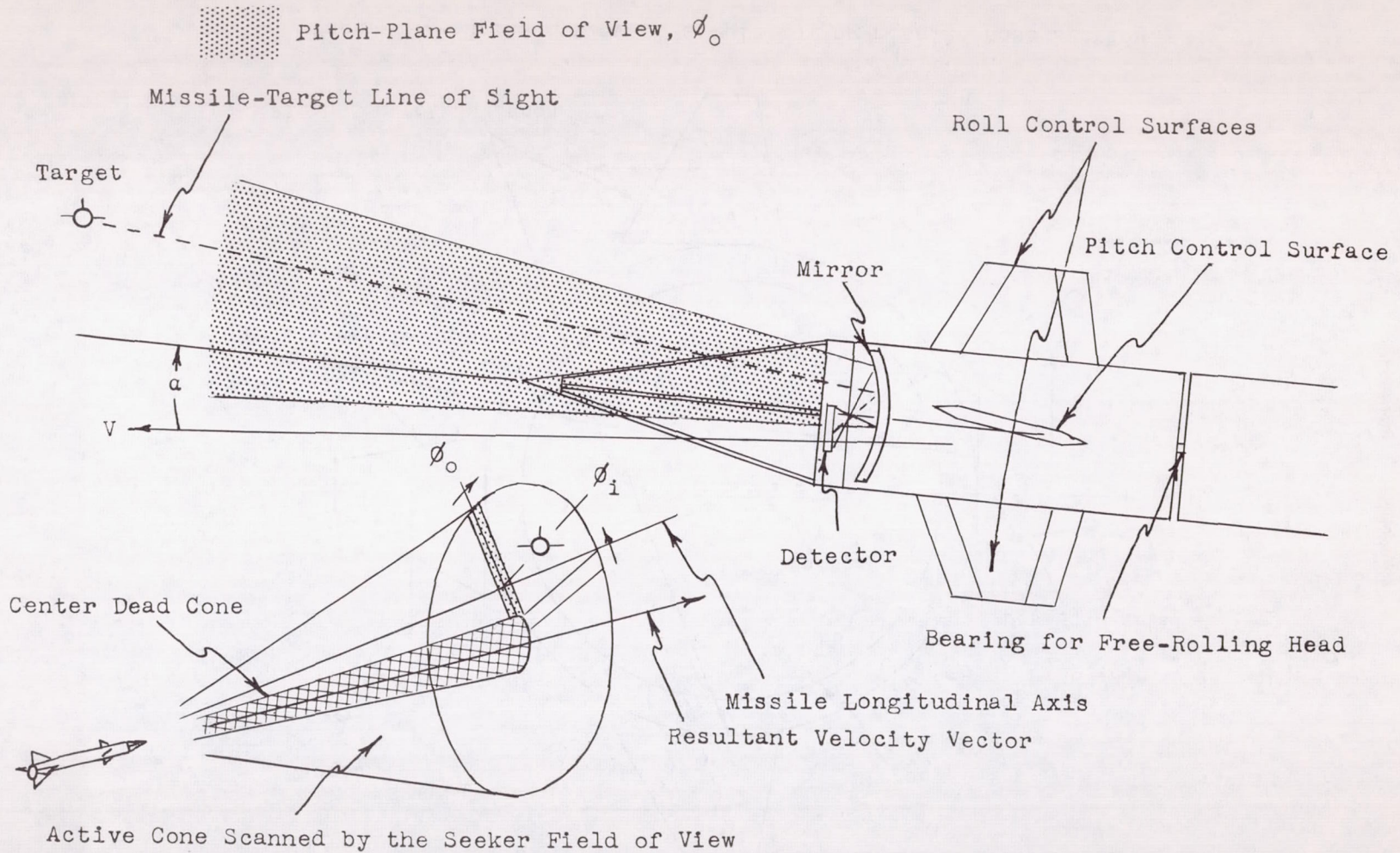
Figure 1.- Schematic diagram of simple homing-missile nose section and
cone scanned by seeker field of view while missile has constant
rolling velocity.
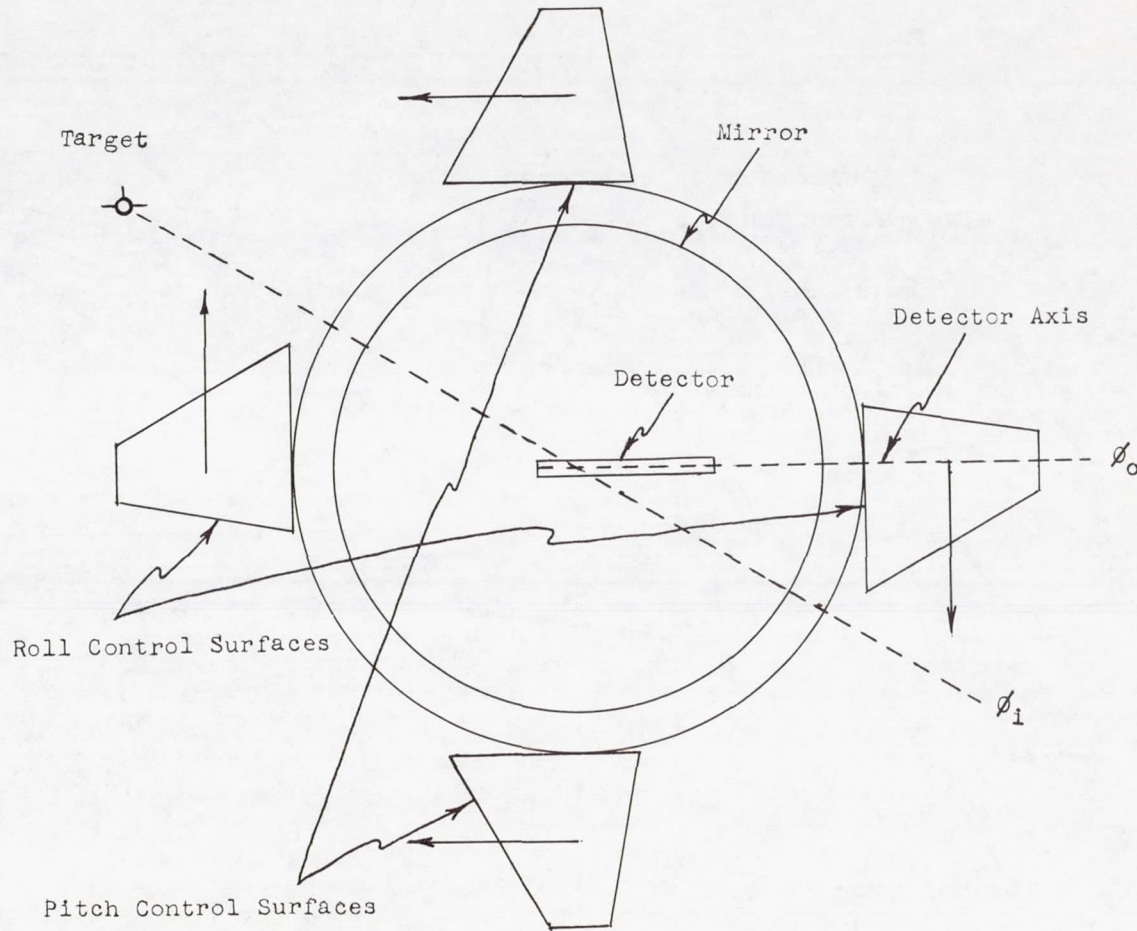
Figure 2.- Head-on view of simple homing-missile nose section.

Homing device

Rocket motor
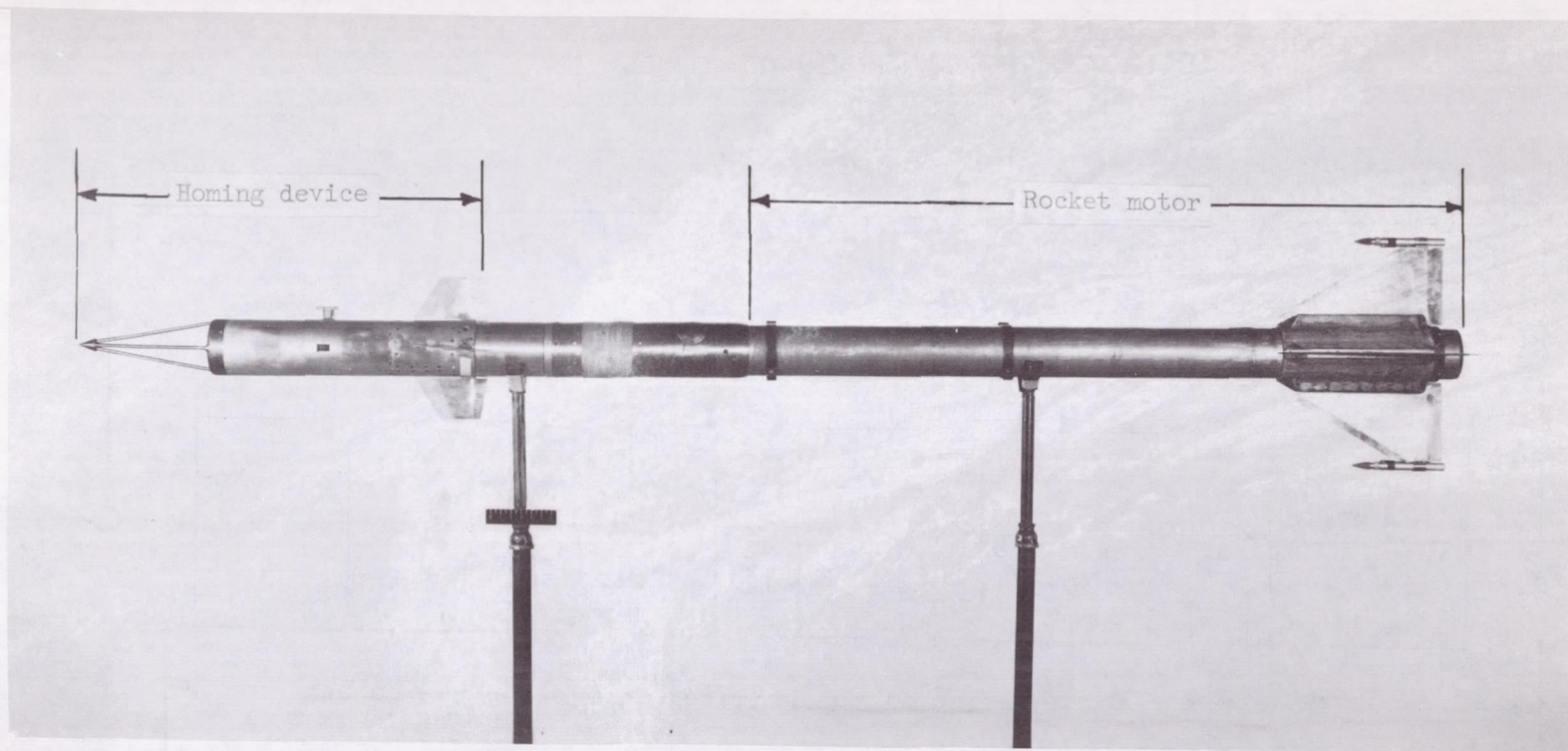
Figure 3.- Simple homing-missile configuration.

L-83480.1
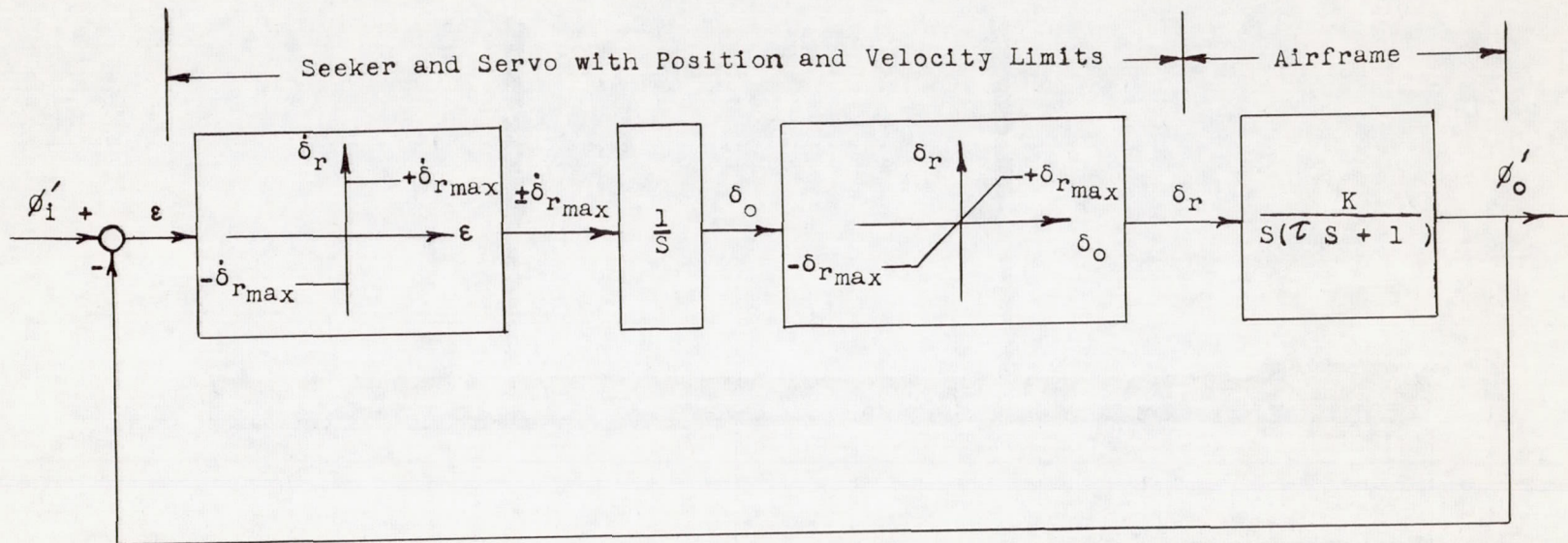
$$\text{Servo Time Delay} = \frac{2 \ \left| \delta_{r_{max}} \right|}{\left| \dot{\delta}_{r_{max}} \right|}$$

Figure 4.- Block diagram of missile nonlinear roll control system.
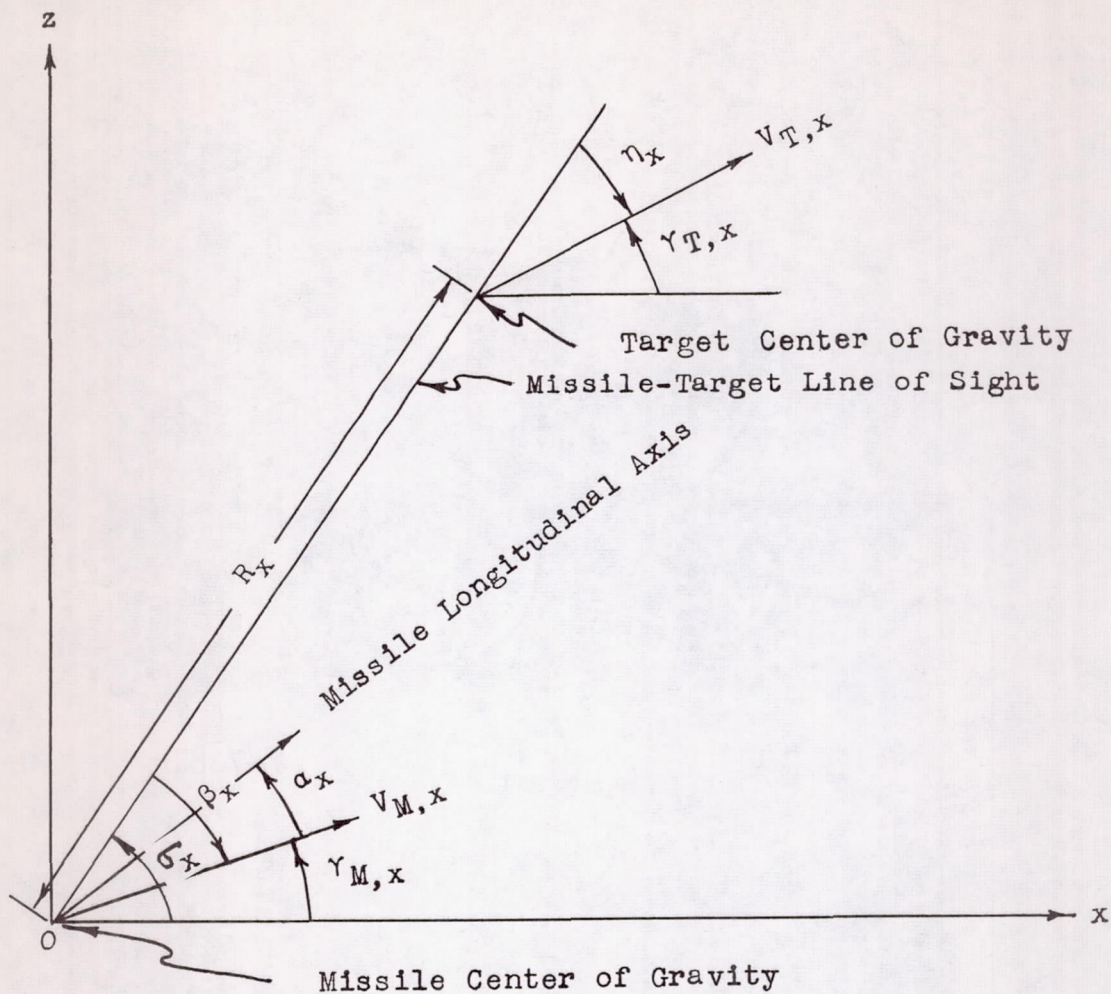
ZX Plane:

$$\dot{R}_x = V_{T,x} \cos \eta_x - V_{M,x} \cos \beta_x$$

$$R_x \dot{\sigma}_x = V_{M,x} \sin \beta_x - V_{T,x} \sin \eta_x$$

$$\sigma_x = \beta_x + \gamma_{M,x} = \eta_x + \gamma_{T,x}$$

XY Plane:

$$\dot{R}_y = V_{T,y} \cos \eta_y - V_{M,y} \cos \beta_y$$

$$R_y \dot{\sigma}_y = V_{M,y} \sin \beta_y - V_{T,y} \sin \eta_y$$

$$\sigma_y = \beta_y + \gamma_{M,y} = \eta_y + \gamma_{T,y}$$

Figure 5.- Missile-target geometry.
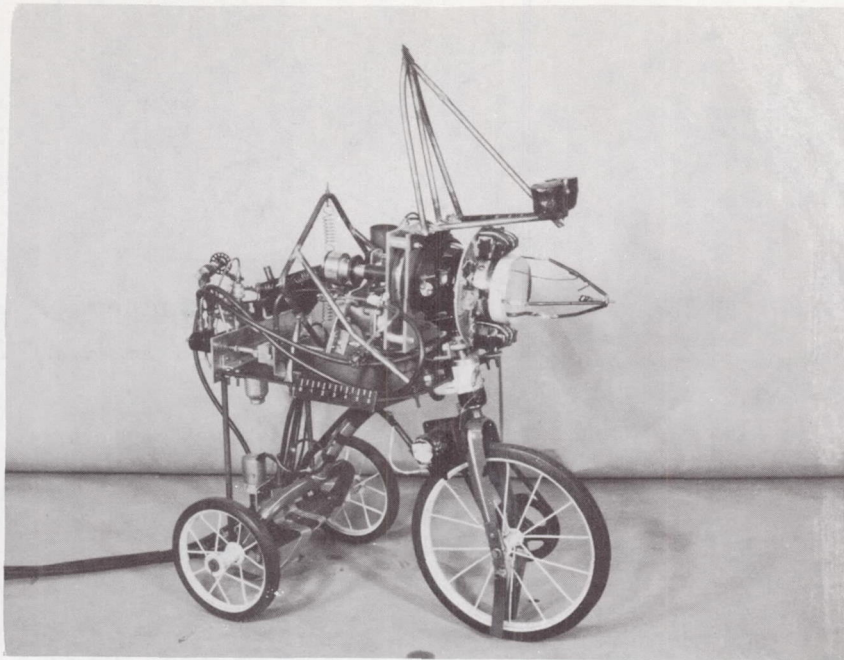
(a) Missile.   L-76824
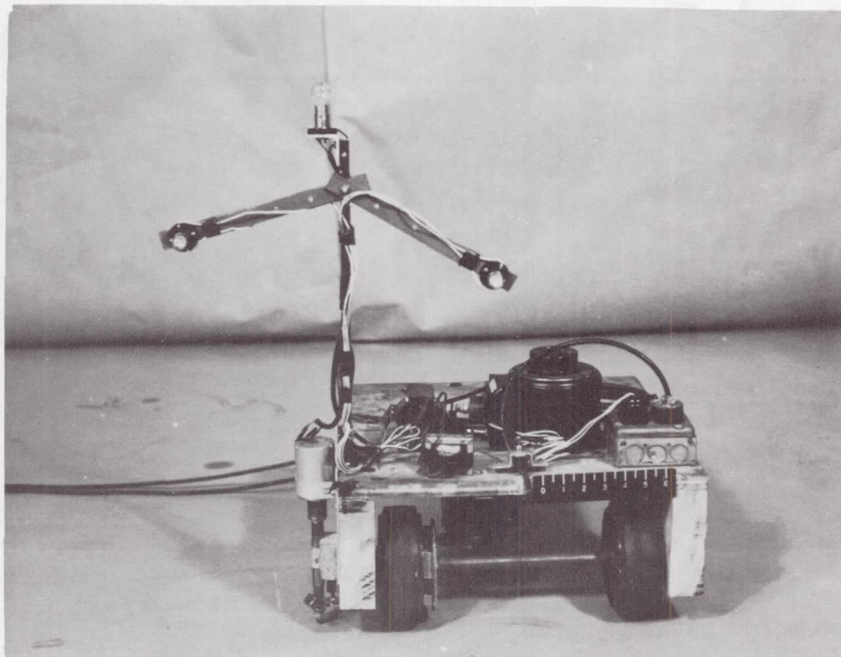
(b) Target.   L-76827

Figure 6.- Qualitative simulator.
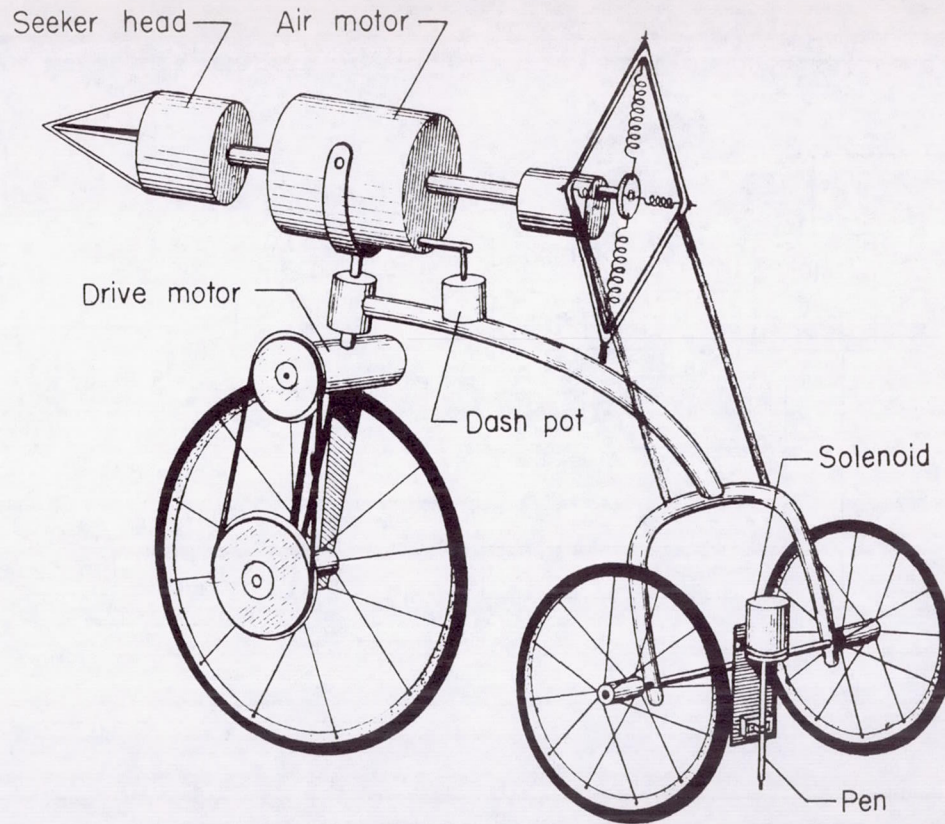
Figure 7.- Functional sketch of missile section of qualitative simulator.
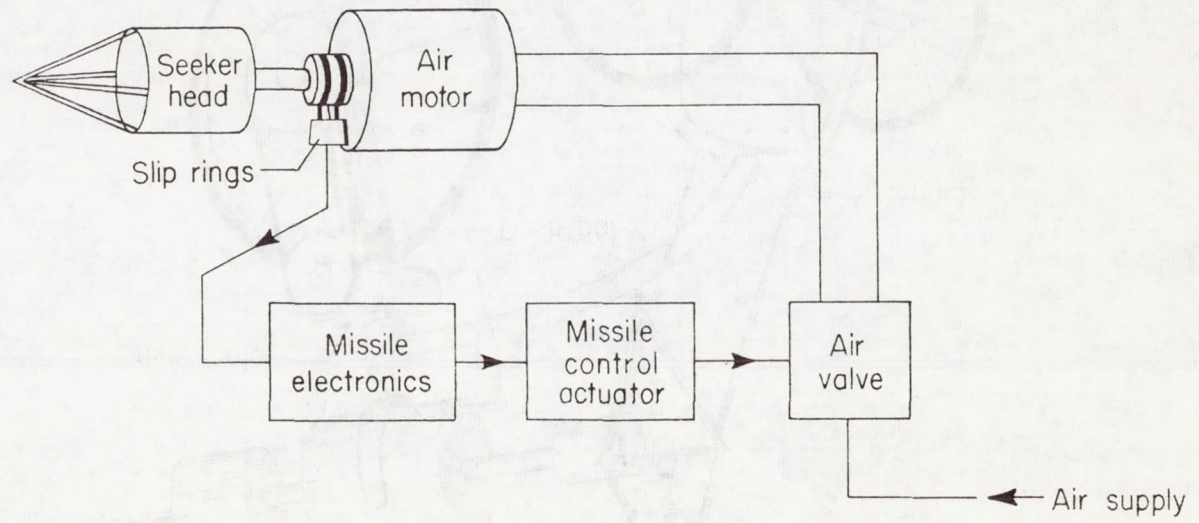
Figure 8.- Block diagram of roll-dynamics unit of qualitative simulator.
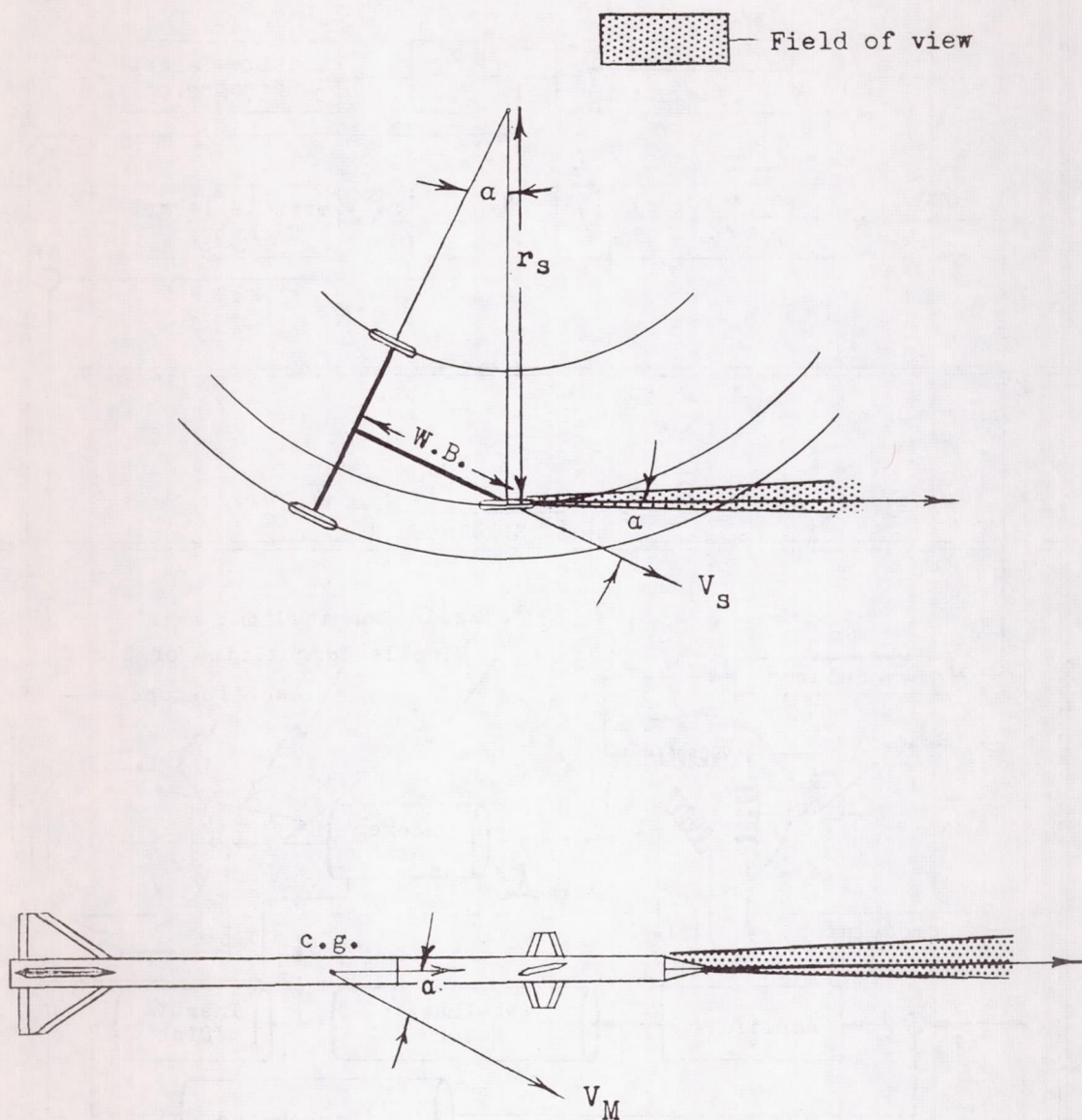
Figure 9.- Steering geometry of qualitative simulator compared with that of missile.

Reeves Analog Computer

$$\delta_y \quad \boxed{\dfrac{K_1}{S^2 + 2\zeta\omega_n S + \omega_n^2}} \quad a_y \quad \boxed{\dfrac{K_2}{S}} \quad \gamma_y \quad \boxed{\text{Missile-Target Geometry}} \quad \beta_y$$

$$\delta_x \quad \boxed{\dfrac{K_1}{S^2 + 2\zeta\omega_n S + \omega_n^2}} \quad a_x \quad \boxed{\dfrac{K_2}{S}} \quad \gamma_x \quad \boxed{\text{Missile-Target Geometry}} \quad \beta_x$$

Roll Simulator

Missile Longitudinal Axis
Missile-Target Line of Sight
Oscilloscope

Demodulator

Resolver

Seeker Head

ϕ_o

Demodulator

$|\delta|$

Amplifier → Two-Phase Motor → Inertia Disk

Tachometer

Time Delay ← "Flip-Flop" and Relay ← Pulse Amplifier
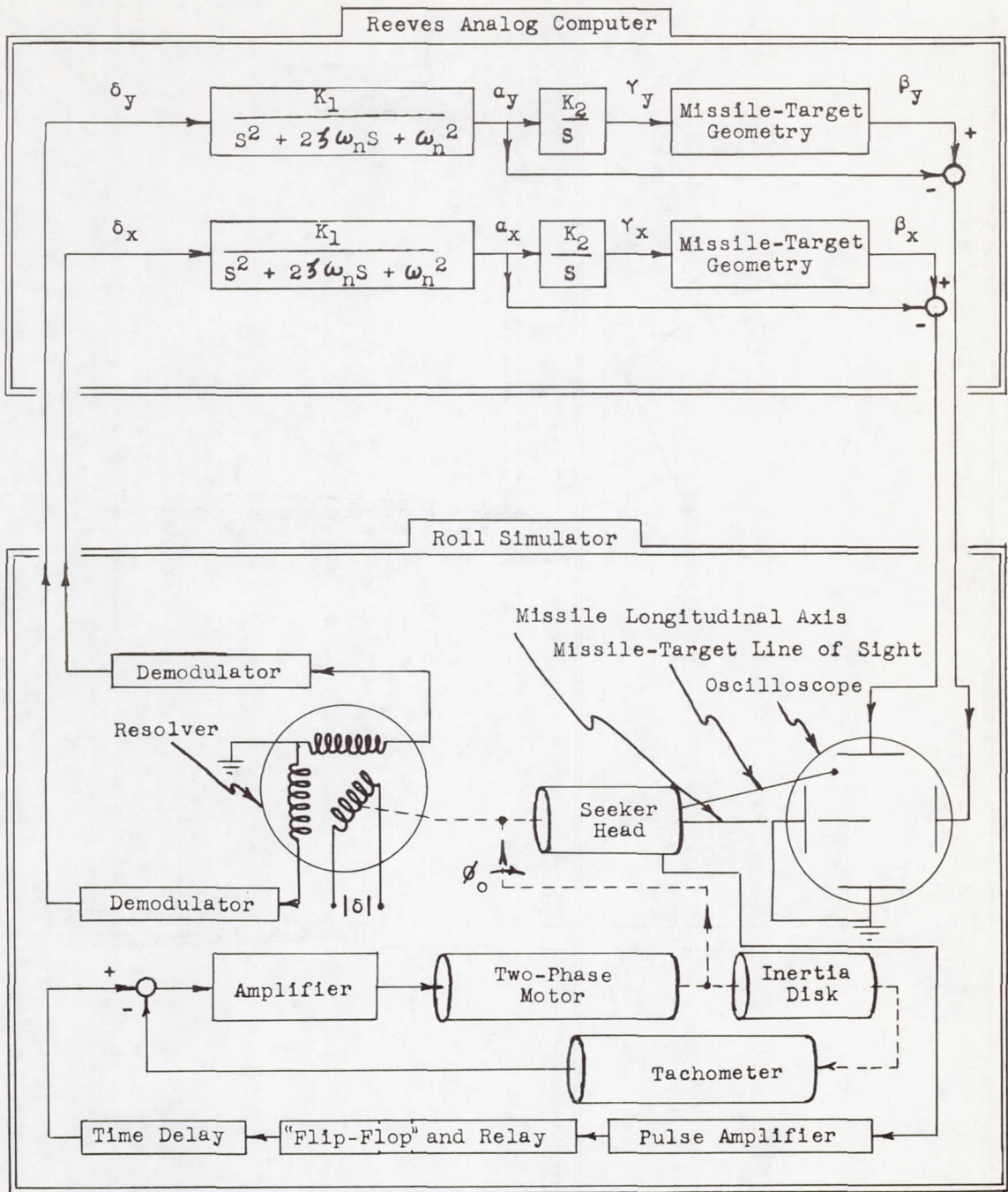
Figure 10.- Schematic diagram of quantitative simulator.
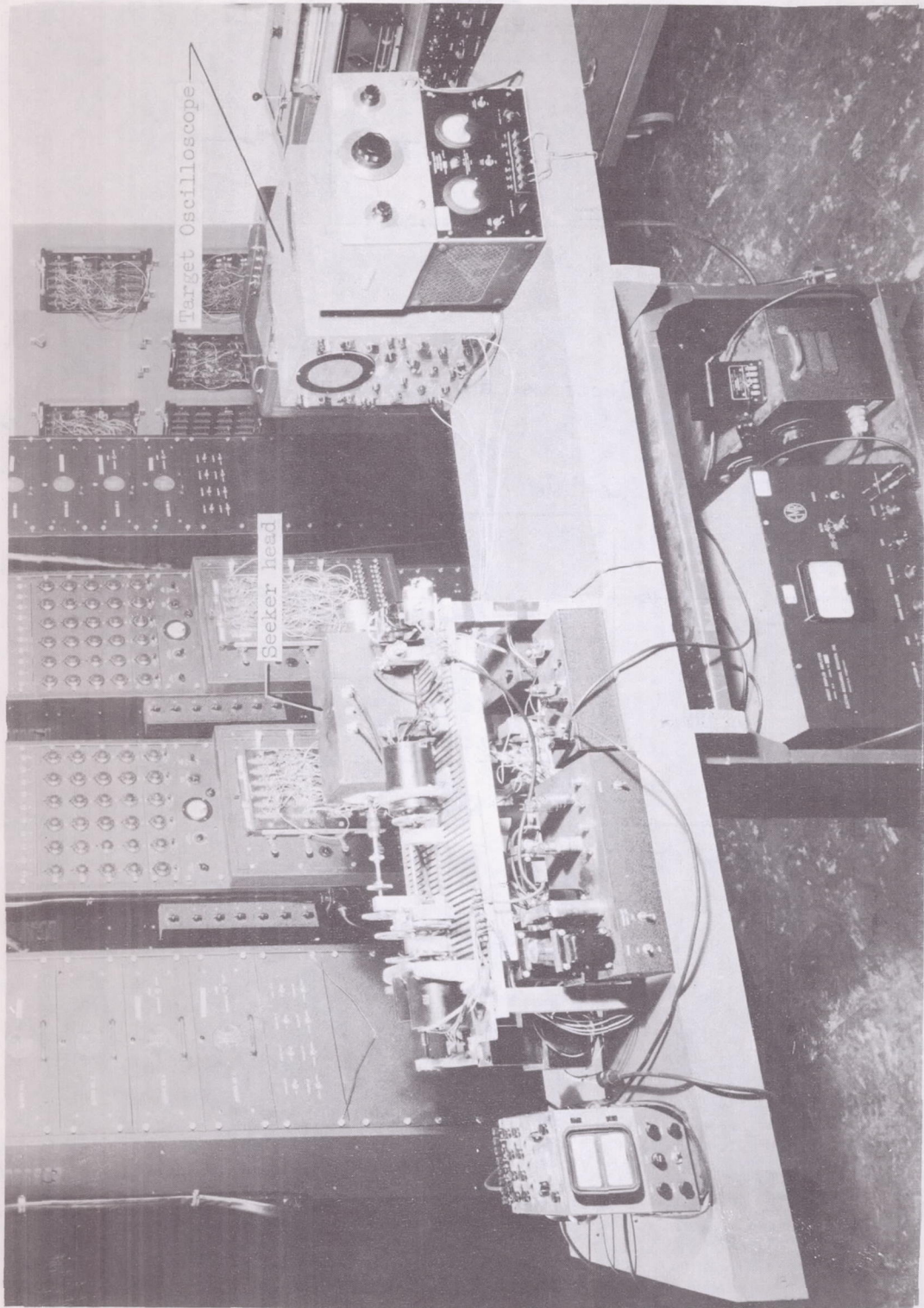
Figure 11.- Photograph of quantitative simulator.   L-78959.1
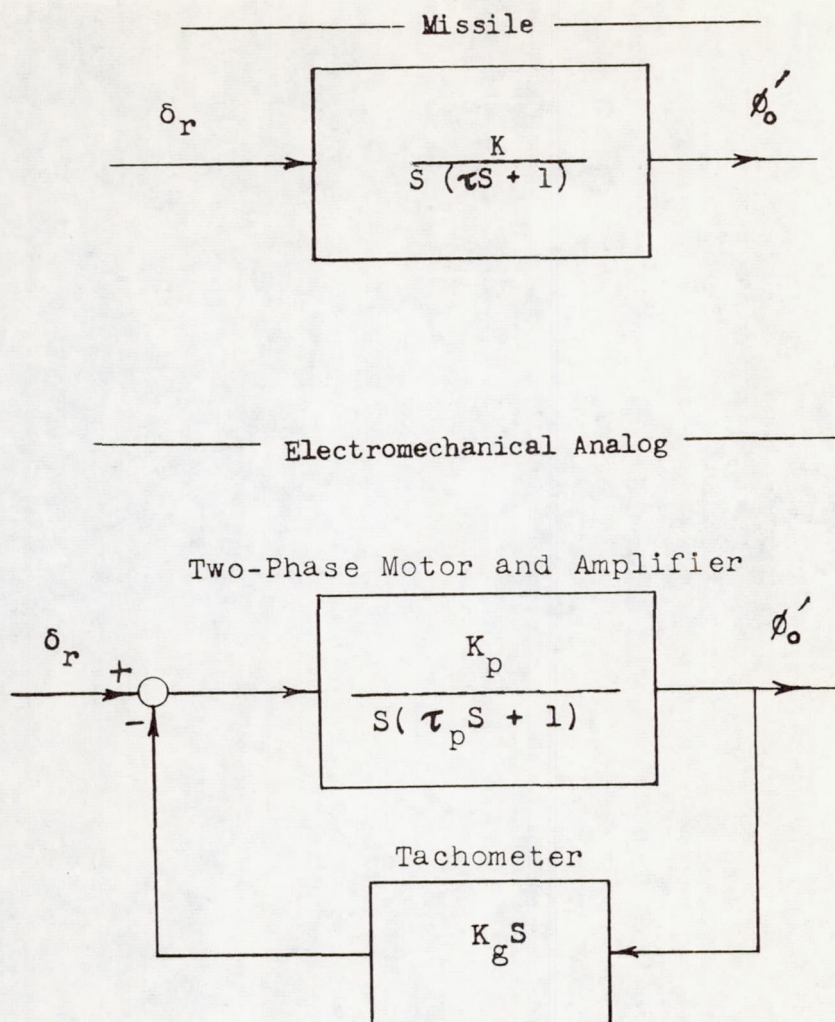
$$K = \frac{K_p}{1 + K_p K_g}$$

$$\tau = \frac{\tau_p}{1 + K_p K_g}$$

Figure 12.- Electromechanical analog of missile roll transfer function.
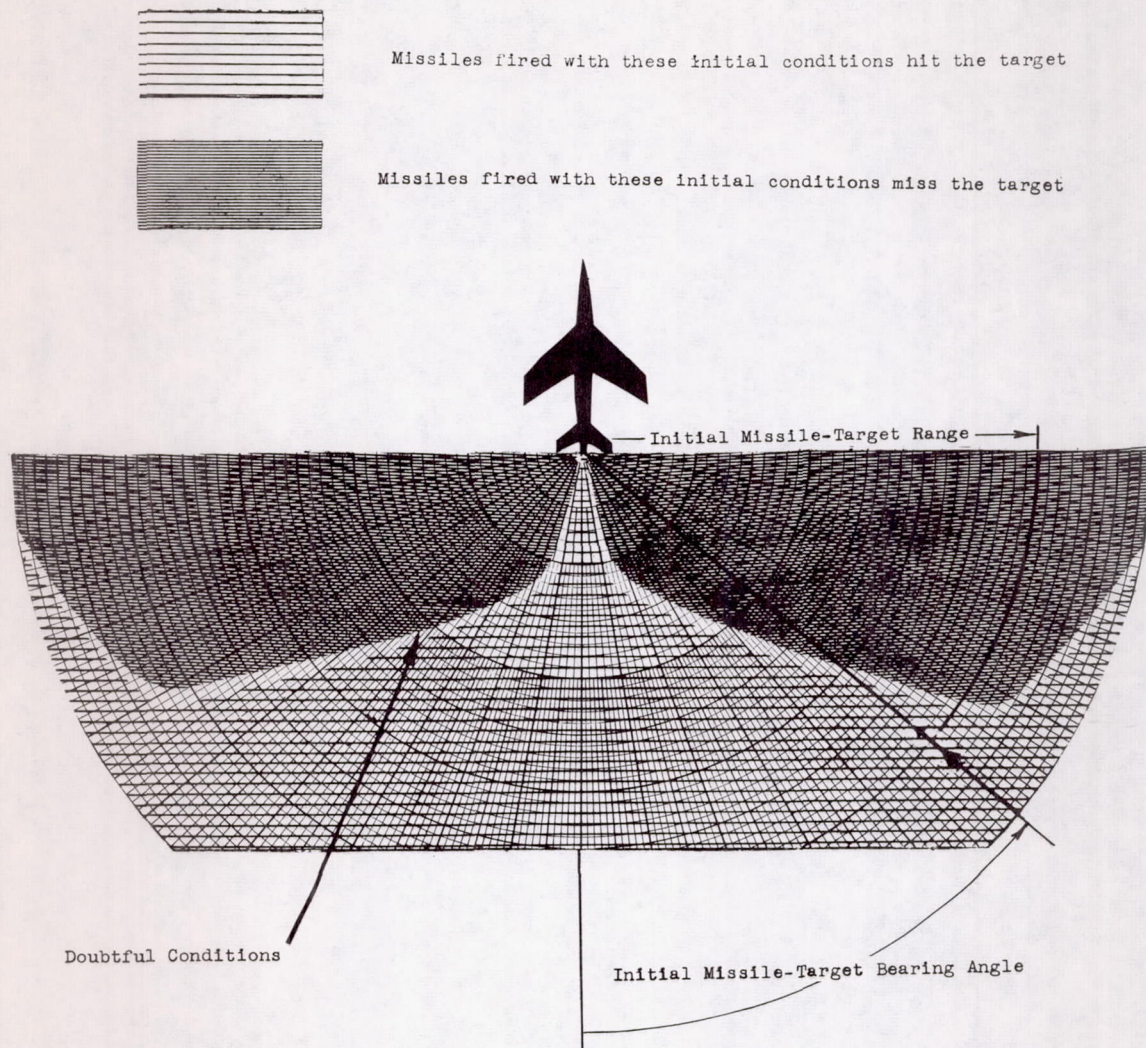
Figure 13.- Diagram illustrating significance of polar plots of initial
conditions necessary for collision.
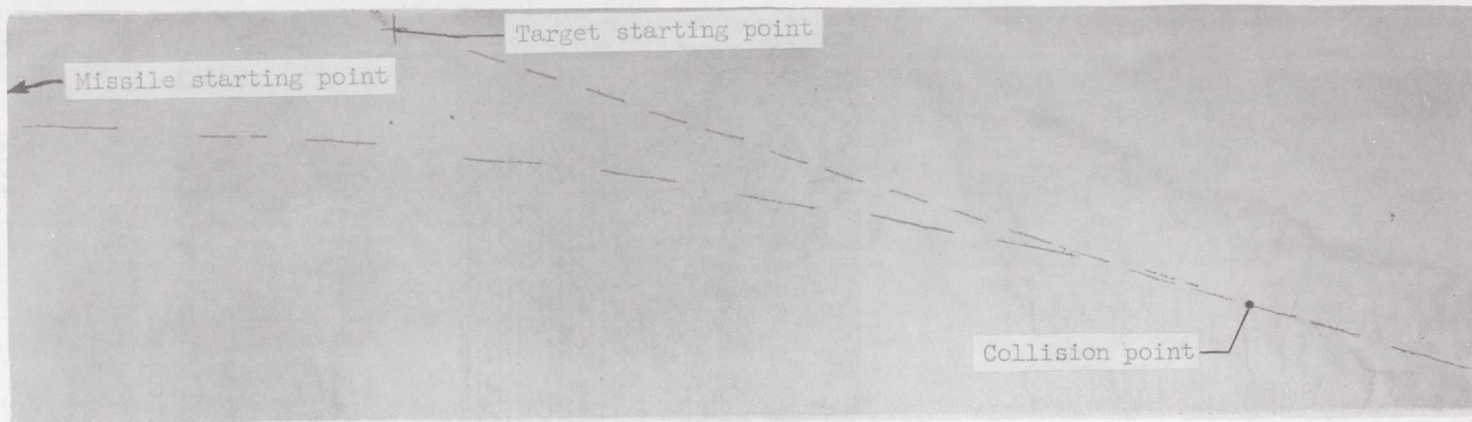
(a) Missile-target bearing angle = 20°.
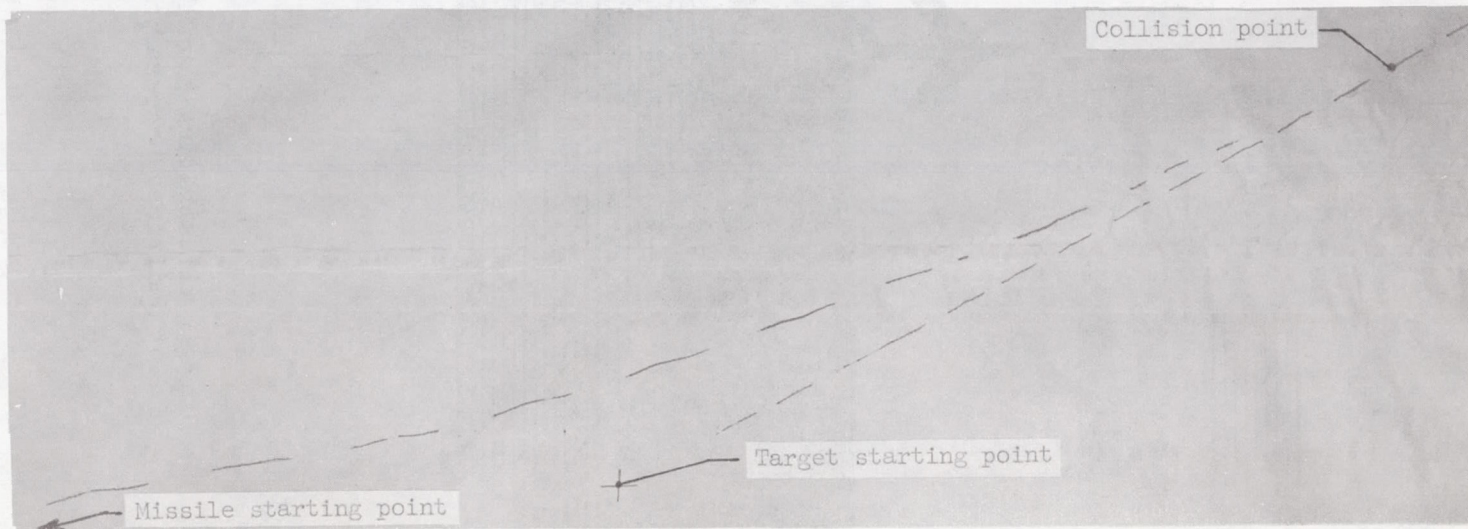
(b) Missile-target bearing angle = 25°.   L-89372

Figure 14.- Qualitative-simulator trajectories simulating missile and
target at M = 1.5 and sea level. Velocity ratio = 2.
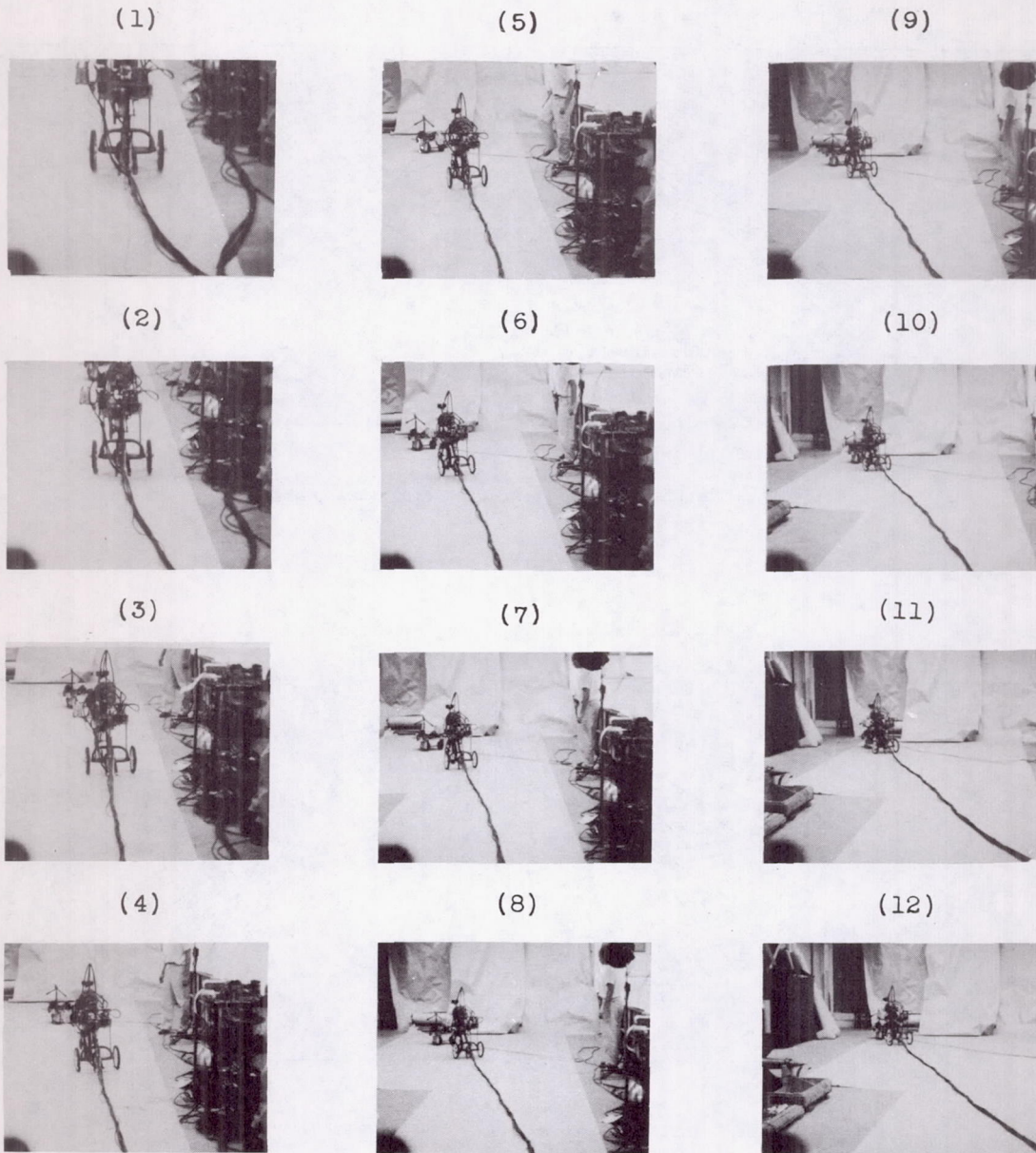
L-89366

Figure 15.- Photographs of qualitative simulator in operation. Initial missile-target range, 2 miles; M = 1.5; sea level; $\eta = 30^\circ$; $\dfrac{V_M}{V_T} = 2$.

$$\frac{a}{\delta} = \frac{541}{S^2 + 8.12S + 884} \qquad \frac{Y}{a} = \frac{3.42}{S}$$

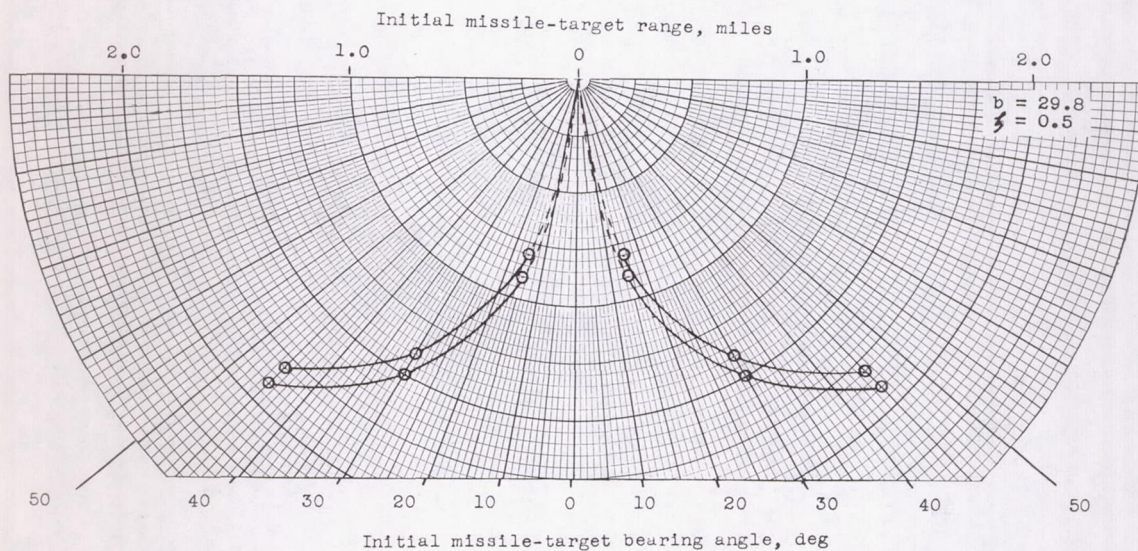Initial missile-target range, miles

(a) Single detector.
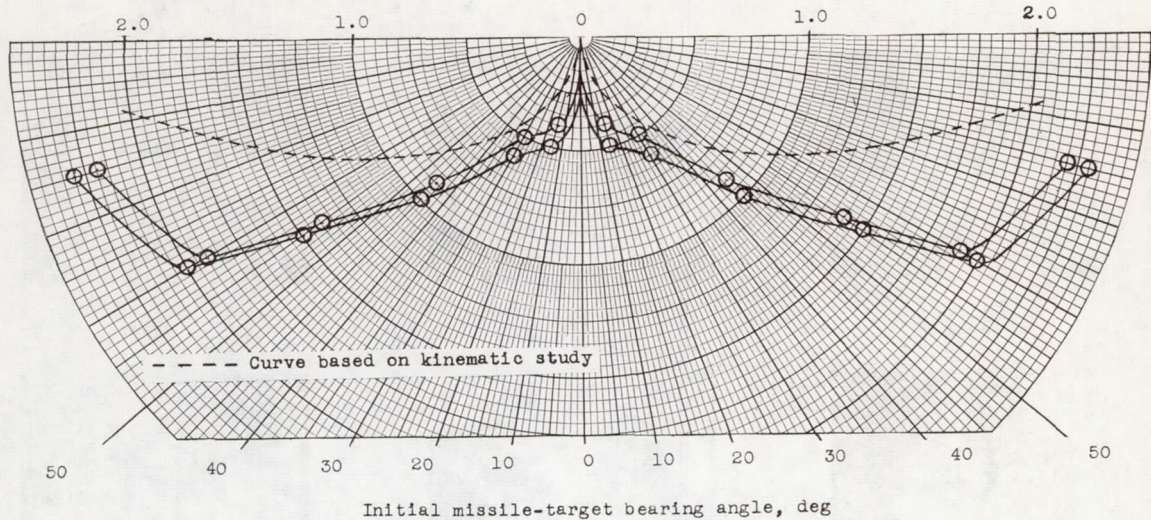
Initial missile-target range, miles
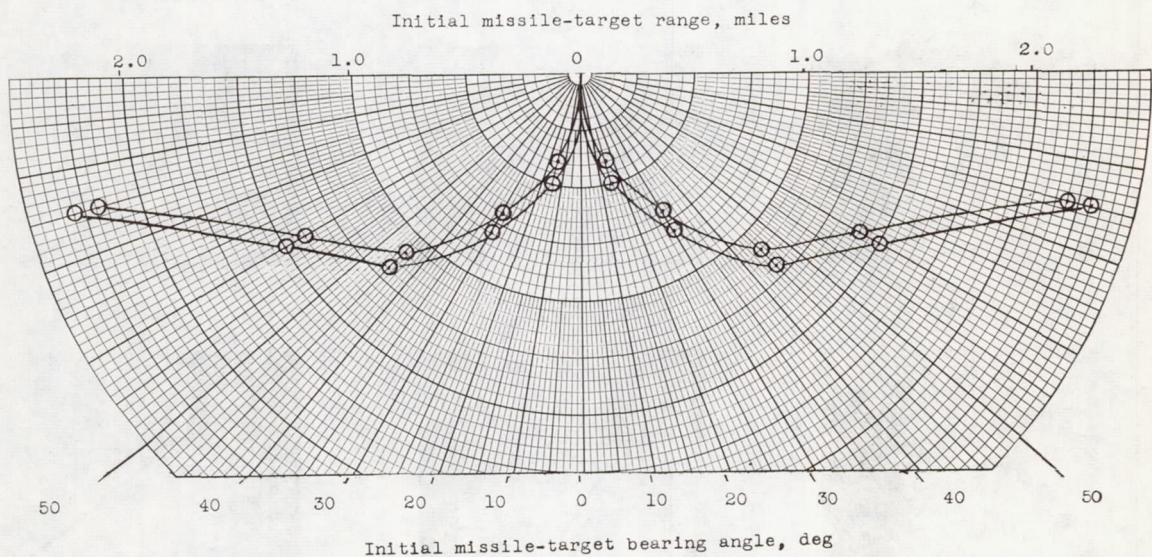
(b) Single detector skewed 10°.

Figure 16.- Polar representation of initial launching range and initial
    missile-target bearing angle necessary for collision. M = 1.2; sea
    level; steady-state roll velocity, 2.7 rps; pitch canard deflection,
    5.2°; servo time delay, 0.02 sec; airframe roll time constant, 0.04 sec;
    $\frac{V_M}{V_T}$ = 2.

$$\frac{a}{\delta} = \frac{541}{S^2 + bS + 884} \qquad \frac{\gamma}{a} = \frac{3.42}{S}$$

Initial missile-target range, miles
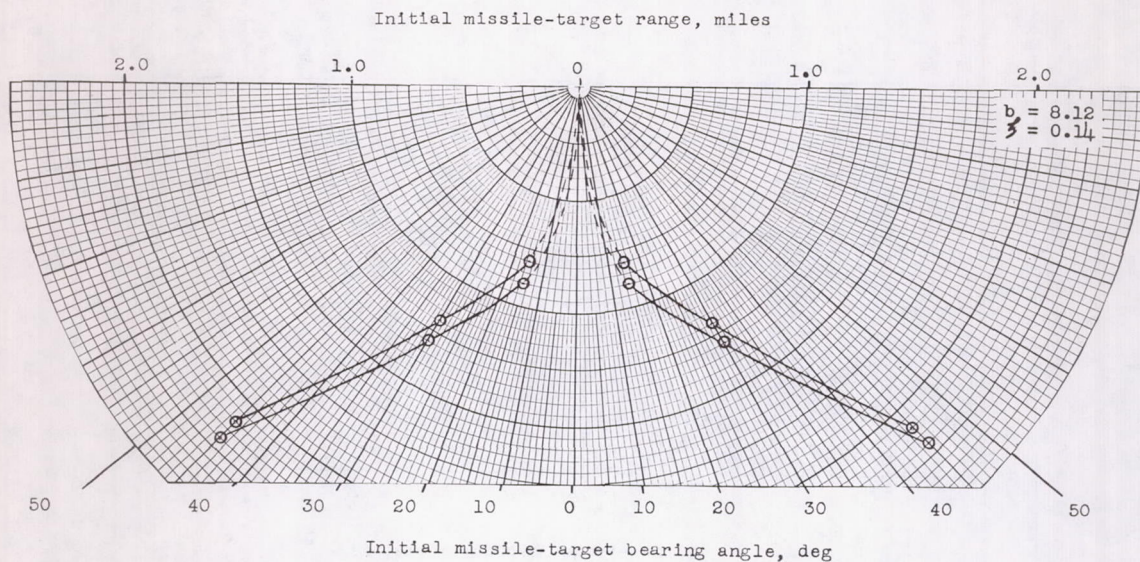
(a) Single detector; b = 8.12.

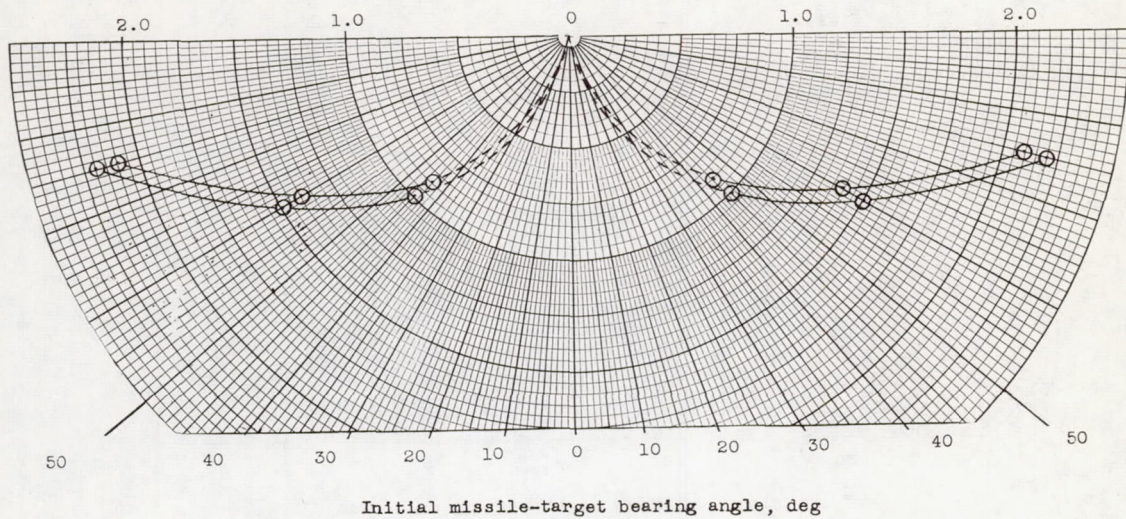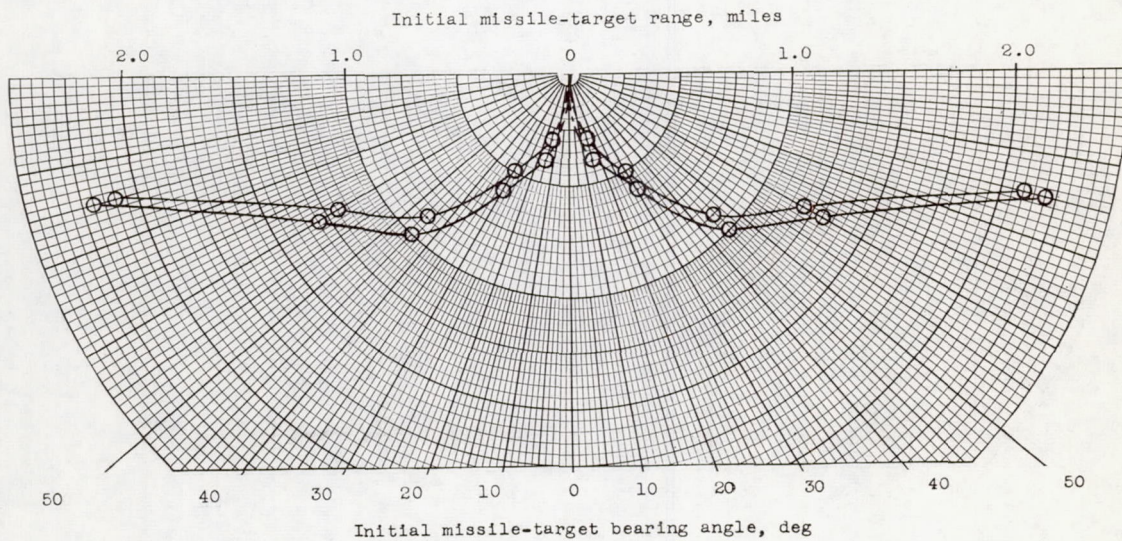(b) Single detector; b = 29.8.

Figure 17.- Polar representation of initial launching range and initial missile-target bearing angle necessary for collision. M = 1.2; sea level; steady-state roll velocity, 3 rps; pitch canard deflection, 5.2°; servo time delay, 0.02 sec; airframe roll time constant, 0.12 sec; $\frac{V_M}{V_T}$ = 2.

$$\frac{a}{\delta} = \frac{.541}{S^2 + 8.12S + 884} \qquad \frac{\Upsilon}{a} = \frac{3.42}{S}$$

Initial missile-target range, miles

Initial missile-target bearing angle, deg

(a) Two detectors angularly displaced 10°.

Initial missile-target range, miles

Initial missile-target bearing angle, deg

(b) Two detectors angularly displaced 20°.

Figure 18.- Polar representation of initial launching range and initial
missile-target bearing angle necessary for collision. M = 1.2; sea
level; steady-state roll velocity, 2.7 rps; pitch canard deflection,
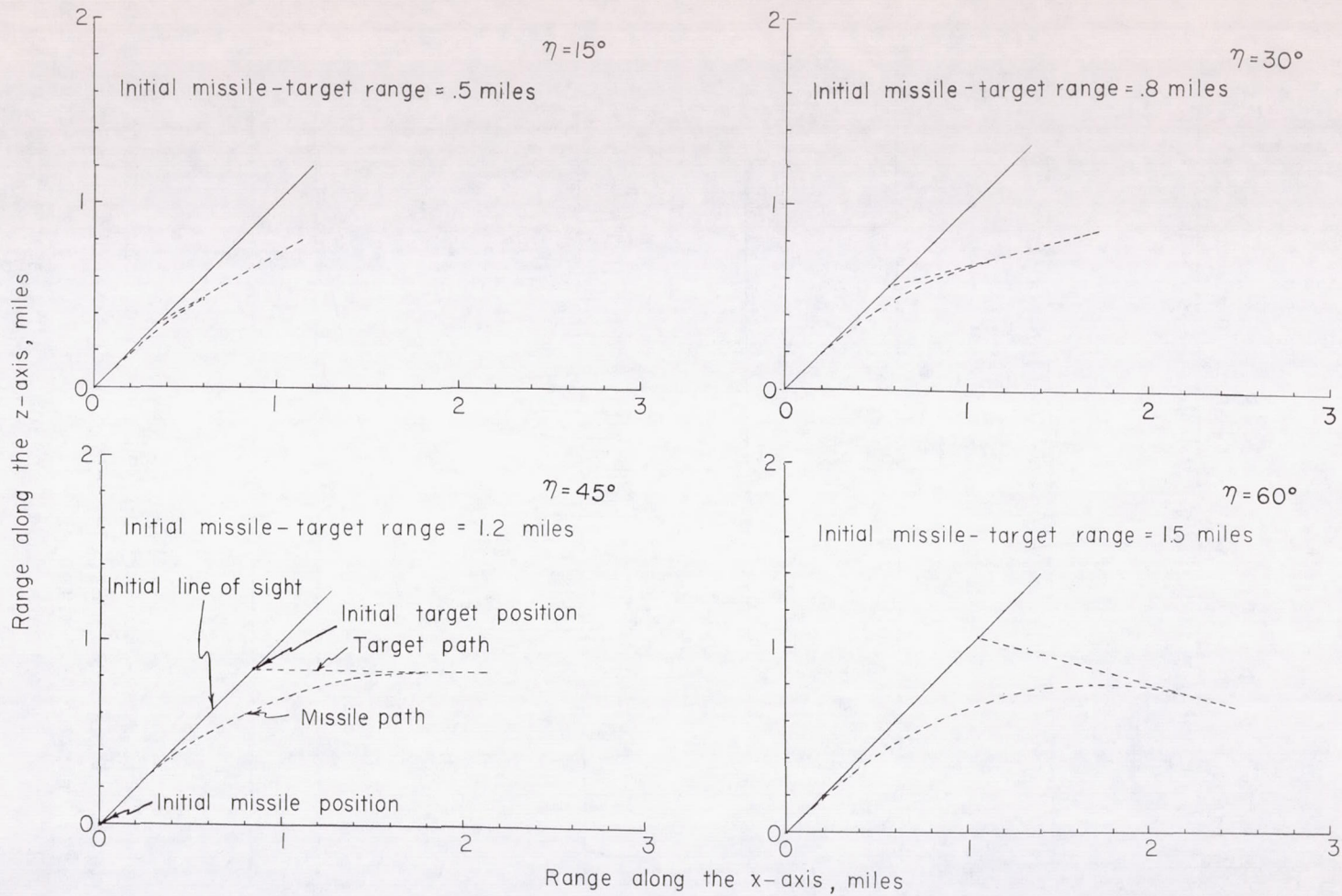5.2°; airframe roll time constant, 0.04 sec; servo time delay, 0.02 sec;
$\frac{V_M}{V_T} = 2$.

Figure 19.- Plots of quantitative-simulator flight paths projected onto xz-plane. Single detector skewed 10°. M = 1.2; sea level; steady-state roll velocity, 2.7 rps; pitch canard deflection, 5.2°; servo time delay, 0.02 sec; airframe roll time constant, 0.04 sec; $\frac{V_M}{V_T} = 2$.
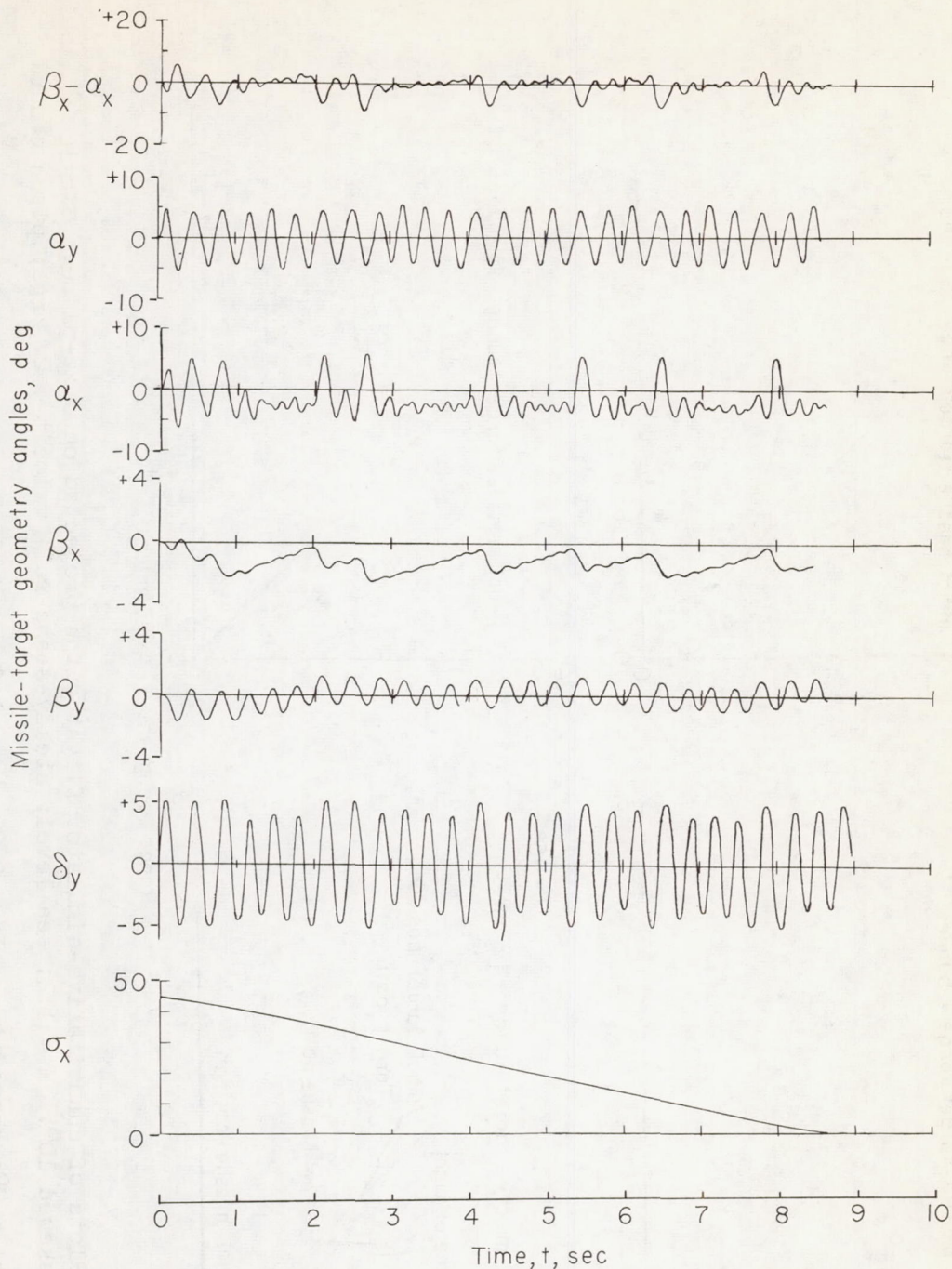
Figure 20.- Missile-target-geometry angles recorded from results obtained on quantitative simulator. Single detector skewed 10°. Initial missile-target range, 1.2 miles; M = 1.2; sea level; steady-state roll velocity, 2.7 rps; pitch canard deflection, 5.2°; servo time delay, 0.02 sec; airframe roll time constant, 0.04 sec; $\frac{V_M}{V_T}$ = 2; η = 45°.